Received: 6 August 2019 | Accepted: 19 November 2019

DOI: 10.1002/hyp.13662

RESEARCH ARTICLE

WILEY

Sustained post-seismic effects on groundwater flow in fractured carbonate aquifers in Central Italy

Lucia Mastrorillo[1] | Michele Saroli[2] | Stefano Viaroli[1] | Francesca Banzato[3] | Daniela Valigi[4] | Marco Petitta[3]

[1]Department of Sciences, University of Roma Tre, Rome, Italy

[2]DICeM-Department of Civil and Mechanical Engineering, University of Cassino and Southern Lazio, Cassino (FR), Italy

[3]Department of Earth Sciences, Sapienza University of Rome, Rome, Italy

[4]Department of Physics and Geology, University of Perugia, Perugia, Italy

Correspondence
Marco Petitta, Department of Earth Sciences, Sapienza University of Rome, Rome, Italy.
Email: marco.petitta@uniroma1.it

Abstract

A sustained increase in spring discharges was monitored after the 2016 Central Italy seismic sequence in the fractured carbonate aquifer of Valnerina–Sibillini Mts. The groundwater surplus recorded between August 2016 and November 2017 was determined to be between 400 and 500 × 10^6 m^3. In fractured aquifers, the post-seismic rise in spring discharges is generally attributed to an increase in bulk permeability caused by the fracture cleaning effect, which is induced by pore pressure propagation. In the studied aquifers, the large amount of additional discharge cannot only be attributed to the enhanced permeability, which was evaluated to be less than 20% after each main seismic event. A detailed analysis of the spring discharge hydrographs and of the water level at five gauging stations was carried out to determine the possible causes of this sudden increase in groundwater outflow. Taking into account the geological and structural framework, a conceptual model of a basin-in-series has been adopted to describe the complex hydrogeological setting, where the thrusts and extensional faults have clearly influenced the groundwater flow directions before and after the seismic sequence. The prevalent portion of the total post-seismic discharge surplus not explained by the increase in permeability has been attributed to changes in the hydraulic gradient that caused seismogenic fault rupture and the disruption in the upgradient sector of the aquifer. The additional flow calculated through the breach of the pre-existing hydrostructural barrier corresponds to approximately 470 × 10^6 m^3. This value is consistent with the total discharge increase measured in the whole study area, validating the proposed conceptual model. Consequently, a shift in the piezometric divide of the hydrogeological system has been induced, causing a potentially permanent change that lowers the discharge amount of the eastern springs.

KEYWORDS

Central Italy, discharge increase, earthquakes, fractured aquifer, hydraulic barrier breaching, permeability enhancement

1 | INTRODUCTION

Hydrogeological responses to earthquakes are very different and include changes in groundwater level (Leggette & Taylor 1935; Cooper, Bredehoef, Papadopulos & Bennett, 1965; Roeloffs, 1998; Brodsky, Roeloffs, Woodcock, Gall, & Manga, 2003; Lachassagne, Leonardi, Vittecoq & Henriot, 2011; Shi, Wang, Manga & Wang, 2015; Barberio, Barbieri, Billi, Doglioni & Petitta, 2017) and variation

in stream flow (Muir-Wood & King, 1993; Manga, Brodsky & Boone, 2003; Montgomery & Manga, 2003; Manga & Rowland, 2009). Modifications of spring features (Wang & Manga, 2015) and changes in temperature and chemical composition of groundwater may also occur (Mogi, Mochizuchi & Kurokawa, 1989; Claesson et al., 2004; Skelton et al., 2014; Kim et al., 2019).Various mechanisms have been proposed to explain the hydrologic responses, including permeability changes in aquifers (Rojstaczer, Wolf & Michel, 1995; Wang, Wang & Kuo, 2004; Manga et al., 2012), permanent changes in static stresses and strains (Muir-Wood & King, 1993; Jonsson, Segall, Pederse & Bjornsson, 2003; Albano et al., 2017), fracturing of geothermal reservoirs (Wang, Wang & Manga, 2004), opening of deep fractures (Sibson & Rowland, 2003), liquefaction (Mohr, Manga, Wang, Kirchner and Bronstert, 2015), breaching of hydraulic barriers or seals (Sibson, 1994; Brodsky et al., 2003), and variations in karst base levels (Saroli, Moro, Gori, Falcucci & Salvatore, 2012).

In detail, earthquakes can produce "transient modifications" of the hydrogeological system (Cooper et al., 1965) and "sustained offsets" that may last a long time after the mainshock (Yan, Woith & Wang, 2014). In summary, the type and intensity of each hydrogeological response to an earthquake depend on the local geological conditions (Manga et al., 2012).

The fractured and locally fissured nature of carbonate aquifers favours a quick co-seismic response in terms of both pore pressure propagation and/or dynamic strain modifications, which may induce temporary changes in permeability (Wakita, 1975; Jonsson et al., 2003). In karst and fractured aquifers, most of the mid- and long-term effects on groundwater flow can be due to the formation of microcracks (Casini, Martino, Petitta & Prestininzi, 2006), unlocking of preexisting fractures and fracture cleaning, and/or fracture dilatancy and closure (Rojstaczer et al., 1995; Elkhoury, Brodsky & Agnew, 2006; Wang et al., 2004; Wang & Manga, 2010). The ultimate effect of all these phenomena is an increase in bulk hydraulic conductivity at the aquifer scale, followed by changes to the hydraulic head, which increases close to discharge zones and correspondingly decreases in recharge areas (Galassi et al., 2014; Wang & Manga, 2015).

Studies of the effects of past earthquakes on the carbonate hydrogeological systems of Central Italy (Esposito, Pece, Porfido & Tranfaglia, 2001, 2009; Carro, Amicis & Luzi, 2005; Amoruso, Crescentini, Petitta, Rusi & Tallini, 2011) generally revealed a strong dependence among hydrogeological anomalies, regional structures, and fault mechanisms. Typically, after the co-seismic peak, the discharge and water table remained at higher values with respect to preseismic conditions for up to several months after the seismic events. This phenomenon was observed after the 1980 Irpinia earthquake in the Caposele spring (Esposito et al., 2001) and after the 2009 L'Aquila earthquake (Adinolfi et al., 2012), and this phenomenon has been explained by the effects of (a) pore pressure propagation due to dynamic stresses caused by seismic waves, which determined the sudden discharge peak, and (b) fracture cleaning, triggered by pore pressure propagation, which induced an increase in bulk hydraulic conductivity of the fractured aquifer (Amoruso et al., 2011). After the three main seismic events of 2016, similar responses have been recorded, and consequently, similar mechanisms have been invoked (Petitta et al., 2018; Rosen et al., 2018; Giacopetti, Fabbrocino, Ianni, Materazzi & Pambianchi, 2019; Albano et al., 2019).

Nevertheless, in the area of the Sibillini Mts., which is very close to the epicentres (<10 km), abrupt changes have been followed by a large sustained increase in discharge over time (approximately +25% of the natural discharge) with respect to the limited magnitude of the seismic events (Valigi et al., 2019). Part of this peculiarity could be explained by the succession of three main events having Mw > 5.5, which repeatedly struck the fractured aquifers. The persistent hydrogeological changes also observed 3 years after the earthquakes cannot be explained by the effects of the increase of the bulk hydraulic conductivity only. In fact, the spring discharges and water-table elevations remained higher for a long time compared with the preseismic conditions, which indicates a continuous additional contribution from the fractured aquifer (Checcucci, Mastrorillo & Valigi, 2017). Consequently, other possible additional factors may have concurred with the observed data, and the post-seismic hydrological response model of the studied area is currently not fully understood.

This paper aims to identify an interpretative mechanism in the Sibillini Mts. area that would explain why the hydrogeological postseismic responses there were larger and longer lasting than the ones usually observed in past earthquakes in the central Apennines. First, the work shows the results of extensive monitoring measurement of the groundwater discharge during and after the 2016 earthquake sequence, exceeding the pre-seismic values. The effect of the enhanced permeability was estimated and deemed insufficient to justify the significantly prolonged and localized overall groundwater discharge in the Sibillini Mts. area. Then, a new conceptual model of the hydrogeological response of carbonate aquifers after an earthquake is proposed and discussed considering the available measurements.

2 | GEOLOGICAL AND HYDROGEOLOGICAL SETTING OF THE STUDY AREA

The Valnerina–Sibillini Mts. (VSM) area corresponds to the southern and external sector of the Umbria-Marchean Apennines (Central Apennines), a northeast verging fold-and-thrust belt, involving the Mesozoic-Tertiary sedimentary sequence. The Triassic evaporites act as the main regional detachment level. This domain consists of a Lower Jurassic carbonate shelf unit overlain by stratified pelagic sediments (Middle Lias–Lower Miocene), with an overall thickness of approximately 2,500–3,000 m (Pierantoni, Deiana & Galdenzi, 2013, and references therein).

The geo-structural framework (Figure 1) can be summarized in an original synorogenic thrust system dissected by subsequent postorogenic extensional faults (Calamita & Pizzi, 1993; Calamita, Coltorti, Farabollini & Pizzi, 1994). The compressive tectonic stage (Messinian to early Lower Pliocene orogenic stage) caused the eastward tectonic overlap of the carbonate units over the foredeep turbiditic deposits (Doglioni, Carminati, Cuffaro & Scrocca, 2007). Limited translational

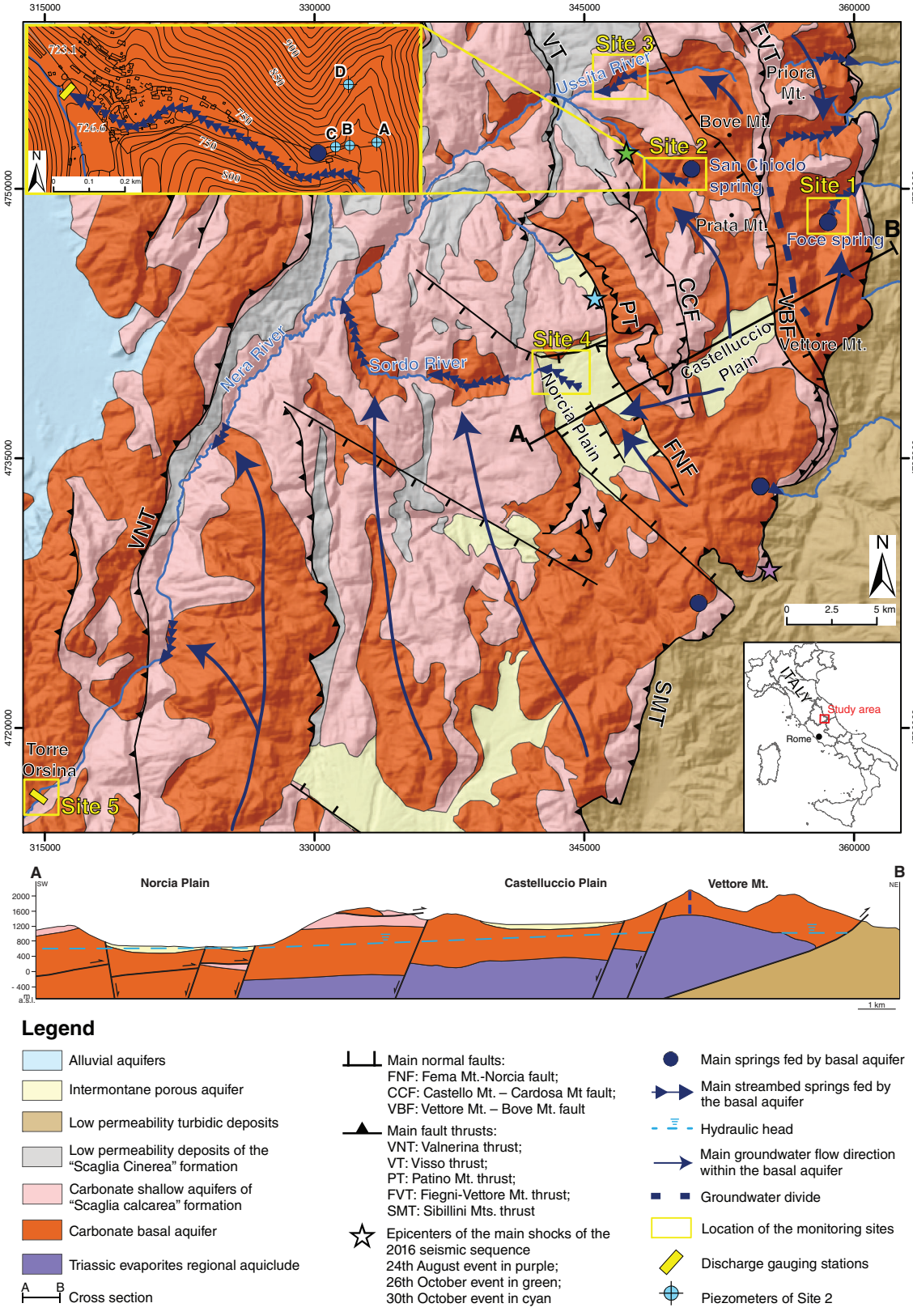

FIGURE 1 Hydrogeological setting of the study area

movements produced a series of asymmetrical NNW–SSE or N–S trending overturned and thrusted eastward folds, with a northward axial plunge (Boni, Mastrorillo, Cascone & Tarragoni, 2005; Centamore, Rossi & Tavernelli, 2009). The following Plio-Quaternary extensional fault stage dissected and/or inverted pre-existing features of the central Apennines fold and thrust belt (Tavani, Storti, Bausà &

Munoz, 2012, and references therein). Western and eastern normal fault systems caused the opening of intermontane extensional basins, subsequently filled with thick continental sequences of Quaternary alluvial, detrital, and lacustrine deposits (Cavinato & De Celles, 1999).

The normal faults, with trends generally at 150°N, are usually characterized by a stratigraphic throw of 100 m, except for Vettore Mt.–Bove Mt. fault (VBF, Figure 1), with a maximum displacement that exceeds 1,000 m (Pizzi & Scisciani, 2000; Pierantoni et al., 2013).

The carbonate units outcropping in the VSM system are the recharge areas of several coexisting aquifers partitioned between shallow and basal regional aquifers (Nanni & Vivalda, 2005; Mastrorillo et al., 2009; Boni, Baldoni, Banzato, Cascone & Petitta, 2010; Mastrorillo & Petitta, 2014). At the regional scale, the basal aquifer is hosted in the Trias–Upper Jurassic formations, whereas several segmented shallow aquifers can be recognized within the Cretaceous limestones ("Scaglia Calcarea", Mastrorillo & Petitta, 2010). A marly–clayey Lower Cretaceous aquiclude is interposed between the two aquifers, preventing groundwater mixing. Generally, the thrust faults act as hydraulic barriers, whereas the normal faults do not necessarily correspond to a groundwater flow seal, because their permeability is controlled by the fracture network properties (connectivity, density, orientation, and length distribution of the fractures) of the fault zone (Bense, Gleeson, Loveless, Bour, & Scibek, 2013; Saroli et al., 2019). The Triassic evaporites underlie the whole groundwater flow, acting as regional bedrock.

The Scaglia Calcarea shallower aquifers (Mastrorillo, 2001) are not analysed in this study, because they are not significantly affected by sustained post-seismic hydrodynamic changes.

The Plio-Quaternary intermountain extensional basins host multilayer porous aquifers mainly fed by lateral inflows from the surrounding carbonate reliefs. These basins mostly act as hydraulic connections between the carbonate fractured aquifers and the rivers flowing in the same intermountain plains. The regional hydrogeological setting is depicted by the hydrogeological cross-section in Figure 1, where the overlay of the shallow aquifer on the basal aquifers was depicted. The Lower Cretaceous marly–clayey aquiclude is not visible at the map scale.

The VSM hydrogeological system is hydraulically sealed by the Valnerina Thrust (VNT; Calamita & Deiana, 1988) along the western side. The Sibillini Mts. Thrust (SMT; Calamita, Cello, Deiana & Paltrinieri, 1994) corresponds to the eastern no-flux boundary of the VSM system. In the studied system, widespread carbonate fracturing ensures infiltration rates from 400 to 1,000 mm/year feeding a total groundwater discharge of approximately 23 m^3/s. The main springs of the area occur in the Nera River basin and along the eastern side of the carbonate system (Figure 1), where 18.2 and 4.6 m^3/s of groundwater, respectively, outflow (Boni, Bono & Capelli, 1986). The basal aquifer feeds approximately 70% of the total discharge of the VSM hydrogeological system, whereas the shallow Scaglia Calcarea aquifers feed the remained rate. The steady rate of springs confirms that groundwater flow is scarcely and only locally influenced by real karst conditions, and at the aquifer scale, the Darcian flow in a fracture network can be considered dominant.

The preferential direction of groundwater flow in the basal aquifer is NNW–SSE or N–S, in accordance with the directions of the fold axis and parallel to the regional structural lineaments, which usually hinder the transversal groundwater exchanges. At the regional scale, the basal aquifer appears to be partially compartmentalized by N–S fault development. In contrast, at the local scale, the same faults can provide non-negligible groundwater seepages, where the fracture

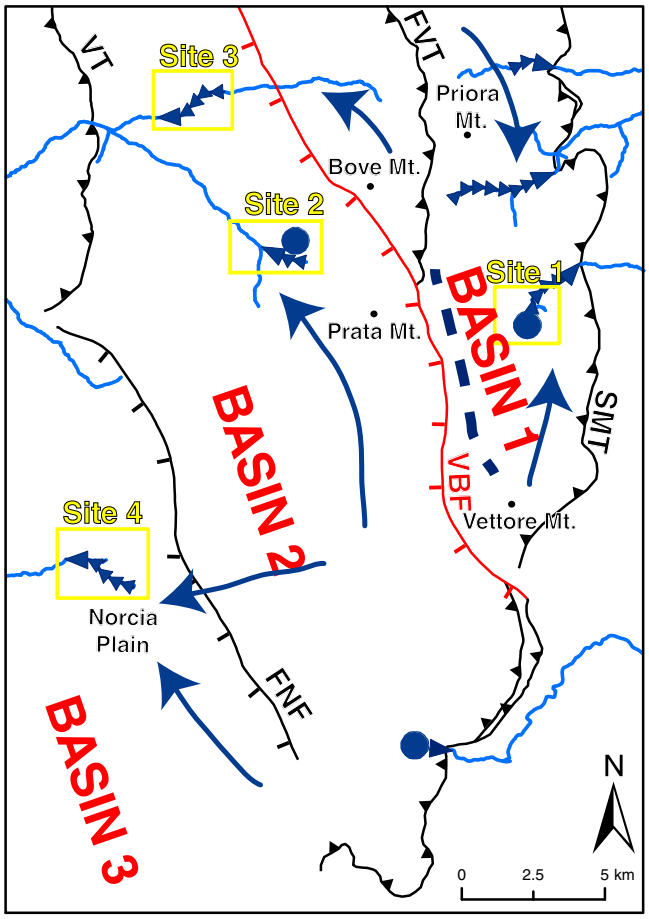

FIGURE 2 Location of the "basin-in- series" of the Valnerina–Sibillini Mts. hydrogeological system and their monitoring sites

network properties allow high permeability conditions. Thus, the VSM system acts as a "basin in series system" (Figure 2), where the whole groundwater flow system is characterized by good interdependence of hydraulic head upgradients and downgradients of low-permeability faults (Petrella, Capuano, Carcione, & Celico, 2009).

The eastern sector of the basal aquifer feeds the baseflow of the rivers at the eastern foot of Sibillini Mts. ridge, at altitudes above 900 m a.s.l. with a discharge of about 2 m^3/s. The western sectors of the basal aquifer drain towards the streambed springs of the Nera River basin between 760 and 250 m a.s.l. for a total discharge of approximately 14 m^3/s. The position of the groundwater divide (Figure 2), which splits the two flow directions, is partially conditioned by the uplift of the bedrock, such that the southern sector of the system has an elevation higher than the water table elevation, as clearly visible in the cross-section of Figure 1.

3 | THE 2016 AMATRICE-NORCIA SEISMIC SEQUENCE

The three main earthquakes of the 2016 sequence (August 24, October 26, and October 30) originated by ruptures nucleated on different segments of the same 40° SW-dipping active normal fault system associated with the 30-km-long VBF (Lavecchia et al., 2016; Tinti, Scognamiglio, Michelini & Cocco, 2016; Huang et al., 2017; Tung & Masterlark, 2018; Brozzetti et al., 2019). This normal fault system almost exclusively crosscuts the middle Lias–Upper Jurassic formations, causing a progressive lifting of the eastern side.

In the study area, coseismic effects during the 2016 sequence have been observed after the main shocks (Pucci et al., 2016; Villani et al., 2019; Luzi, D'Amico, Massa & Puglia, 2018; Liberatore, Doglioni, AlShawaa, Atzorib & Sorrentino, 2019), and several numerical modelling approaches based on the seismological data collected have been produced (Cheloni et al., 2017; Valerio et al., 2018; Walters et al., 2018). The results agree that each main shock caused surface faulting along the ~28-km-long VBF fault system as follows:

- The August 24 earthquake (Mw 6.0) ruptured two distinct segments, one of which corresponds to the southern part of the VBF, and nucleated at a depth of 8 km. The maximum fault slip is located approximately at 3–4 km at depth and reaches the surface only in the section of the M. Vettore for a length of approximately 4–5 km (Chiaraluce, Valoroso, Piccinini, Di Stefano & De Gori, 2011; Bigi, Casero, Chiarabba, & Di Bucci, 2012; Cheloni et al., 2014 and 2017; EMERGEO Working Group, 2016).
- The October 26 Mw 5.9 event activated the northern ~15-km-long segment of the VBF at a depth of ~4 km (Chiaraluce et al., 2017; Civico et al., 2018; Cheloni, Falcucci & Gori, 2019).
- The October 30 Mw 6.5 main shock ruptured the ~20-km-long segment of the VBF that remained unbroken after the previous events. The slip reaches the surface in the area where surface ruptures have been observed. The average offset calculated from variable slip modelling in the elastic field and from field surveys (Cheloni et al., 2017, 2019; Galadini et al., 2017; Civico et al., 2018; Brozzetti et al., 2019) is approximately 0.775 m, which is related to the mean water table depth of the basal aquifer.

The pattern of the deformation caused by this seismic sequence has been interpreted by different slip models. Some dissimilarities in terms of accurate fault location, fault size, fault dip angle, and slip distribution along the ruptured plane (Coltorti & Farabollini, 1995; Pierantoni et al., 2013) suggest that models based on a single planar fault slipped in the October 30 earthquake may not be exhaustive (Cheloni et al., 2017; Chiaraluce et al., 2017; Pizzi, Di Domenica, Gallovic, Luzi & Puglia, 2017; Scognamiglio et al., 2018; Valerio et al., 2018; Walters et al., 2018; Cheloni et al., 2019).

4 | THE MONITORING SITES

Five representative monitoring sites were chosen in the study area representing the main aquifer sectors included in the VSM system (yellow boxes in Figure 1). Four of these sites monitor groundwater discharge outflowing from each "basin in series" (Figure 2), and the fifth is the Torre Orsina gauging station (TO) along the Nera River, where the total spring discharge of the western sector of the VSM hydrogeological system can be monitored. The pre-seismic minimum and mean values of the annual discharge recorded at each monitoring site are summarized in Table 1.

Site 1 corresponds to the highest outflow from the basal aquifer on the eastern side of the VSM system (Foce spring with a mean discharge of 0.5 m^3/s). It is part of a large 50 km^2 aquifer (Basin 1) that is laterally limited by the SMT along the eastern boundary and by the Fiegni–Mt.Vettore Thrust (FVT) and the groundwater divide along the western side. The total discharge of the aquifer is 1.42 m^3/s and is fed by a groundwater flow with prevailing N–S direction (Mastrorillo et al., 2012).

Site 2 (Upper Nera River) and Site 3 (Ussita River) monitor the discharge of two streambed springs located in the Bove Mt.–Prata Mt. aquifer (Basin 2) bounded at the east by the FVT and the groundwater divide. The southern part of this aquifer has a local hydraulic connection with the neighbouring western basal aquifer (Basin 3) through the segment of the Fema Mt.–Norcia Fault (FNF) skirting the Norcia Plain (Petitta, 2011). The whole estimated recharge area of this aquifer is approximately 97 km^2, with the main groundwater flow northward oriented. The total mean discharge of the aquifer is approximately 2.00 m^3/s, 1.30 m^3/s of which flows out in the Nera River near the San Chiodo tapped spring and the remaining 0.70 m^3/s flows out along the Ussita River (Boni et al., 2010), exactly where the monitoring sites are located.

Site 4 (Sordo River) is located in the Norcia Plain aquifer (Basin 3), whose boundaries are still not clearly identified. The mean discharge measured in Site 4 (1.59 m^3/s) corresponds to the total discharge of the aquifer, which corresponds to a recharge area of at least 65 km^2. The piezometric surface of the Norcia Plain highlighted two different

TABLE 1 Minimum, mean discharge and standard deviation of the discharge detected at the five monitoring sites before the 2016 seismic events

Monitoring site	Elevation (m a. s.l.)	Start of the reference period	Minimum discharge (m^3/s)	Mean discharge (m^3/s)	Standard deviation (m^3/s)
1. Foce Spring	910	January 4, 2009	0.32	0.57	0.03
2. Upper Nera River	750	January 1, 2011	0.74	1.30	0.35
3. Ussita River	607	January 9, 1991	0.37	0.69	0.21
4. Sordo River	555	April 26, 1990	0.94	1.59	0.18
5. Nera River (TO)	210	January 1, 2006	12.28	20.03	5.60

flow directions: partly from the south and partly from the east, through the FNF (Petitta, 2011).

Site 5 corresponds to the Torre Orsina (TO) gauging station and is located along the Nera River at the exit of the VSM system. The TO gauging station closes a 1,445 km^2 wide catchment, including the drainage basins of the gauging stations of Sites 2, 3, and 4. The average Nera River discharge recorded in the 2006–2018 period is approximately 20 m^3/s, which is more than 90% fed by the discharge of all upstream springs in the catchment, with a negligible contribution of runoff. Most of the Nera River baseflow was fed by the spring discharge of the basal aquifer (at least 78% according to Mastrorillo et al., 2009). In this context, Site 5 seems to be an adequate tool to evaluate the basal aquifer discharge regime of the western sector of the VSM hydrogeological system. The groundwater mean discharge measured in Sites 2, 3, and 4 corresponds to approximately 17% of the baseflow measured in Site 5 according to the data shown in Table 1.

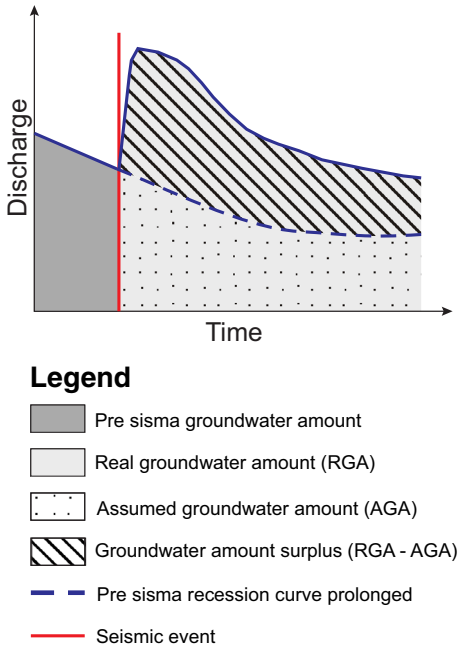

FIGURE 3 Subdivisions of the groundwater amount within a discharge hydrograph affected by earthquake

5 | METHODOLOGY

The data from the five monitoring sites were collected by the Hydrographic Services of the Umbria Region, water supply companies or directly from the research team. In Site 1, the spring discharge is measured in the tunnel drainage of the local water-supply system by automatic water level sensors and converted into discharge through the related rating curve. Sites 2, 4, and 5 are equipped with pressure probes or automatic ultrasonic measurement sensors. Rating curves have been used in conjunction with river stage measurements to determine the river discharges. Only in Site 3 was the river discharge unevenly measured using a portable flow meter. Additionally, the water-table depths were recorded in four piezometers of Site 2 by downhole data loggers with atmospheric compensation.

The complete time interval of the data set is reported in Table 1. A uniform and synchronous time series of discharge data, from January 1, 2016, to December 30, 2017, was analysed in this study. Data processing was performed daily, but hourly frequency data were also processed when necessary.

The hydrograph recession analysis (Maillet, 1905) was carried out to analyse groundwater discharge and water table heads over time, to compare the volume of groundwater discharge outflowed after a seismic event ("Real groundwater amount," RGA) with the expected volume in the absence of an earthquake ("Assumed groundwater amount," AGA). The difference between the RGA and AGA provides a quantification of the amount of groundwater mobilized by the earthquake sequence (Figure 3).

The persistence of the low flow condition, due to the 2016–2017 drought period (IRSA-CNR, 2017), allowed us to set the end of the period considered at the end of the hydrograph depletion curves recorded at the gauging stations (November 30, 2017).

In cases where the recession curve is not clear, due to the steadiness of the spring regime (Sites 1 and 4), the AGA was taken as the value of the pre-seismic average discharge.

Three main seismic shocks occurred in 2016 (August 24, October 26, and October 30), but the two events in October occurred very close in time; therefore, it is not possible to distinguish their different

effects. The analysis of the hydrogeological effects recorded between October 26 and 30 are therefore not meaningful. The evaluations were made for both periods August 24 to October 26, 2016, and October 30, 2016, to November 2017, to discriminate between the effects of the first and the third event. The effects of the third event are not exclusive and may also include some effects from the first event that are not fully exhausted.

The persistence time of the earthquake effects on the hydrogeological features was also calculated by extending the calculated recession curve on the discharge outflowed after the seismic events until reaching the pre-earthquake average conditions.

The time trend of the hydraulic gradient during pre- and post-seismic conditions was reconstructed from data recorded in the Site 2 piezometers (Figure 1). Two hydraulic gradient hydrographs were reconstructed between three intermediate piezometers (A, B, and C) located along the EW groundwater flow direction. A third gradient hydrograph was calculated between the highest piezometer (D) and San Chiodo spring (located along the Upper Nera riverbed at 750 m a.s.l.), along the NS flow direction. The mean hydraulic gradient hydrograph was obtained by the daily average of the gradients considered.

The enhanced permeability was estimated from the comparison between Site 2 discharge and the hydraulic gradient calculated between the D piezometer and San Chiodo spring. The estimation is based on the Darcian flow model, whereby the discharge increase is linked to both enhanced permeability and hydraulic gradient rise. For each of the two events, the portion of the hydrograph in which discharge increase is not associated with gradient rise analysed in detail. On the first approximation, we could attribute this discharge increase to the enhanced permeability due to the earthquake and estimate the relative rise of the bulk hydraulic conductivity. When the hydraulic gradient begins to rise, it is no longer possible to distinguish the enhanced permeability effect because the increase in recharge is clearly affected by the rise in hydraulic gradient.

6 | RESULTS

The elaboration of the daily discharge data produced the hydrographs shown in Figure 4. By focusing on the hydrogeological long-lasting changes, only Site 1 produced a significant discharge decrease over time and produced a final discharge much below the pre-seismic mean value. Conversely, the discharges of Sites 2, 3, and 4 substantially increased, remaining higher than the pre-seismic mean values. The final discharge result of Site 5, despite the great increase of the previous months, is equal to the pre-seismic mean value.

The effects of the August event on the increase in discharge seem to be transient at all sites, except Site 4, where a gradual and sustained increase in discharge is evident during the intermediate period between the two main seismic events. In contrast, in the other cases, a slight discharge drop was recorded.

The October events affect the discharge with different consequences, as follows (Figure 4):

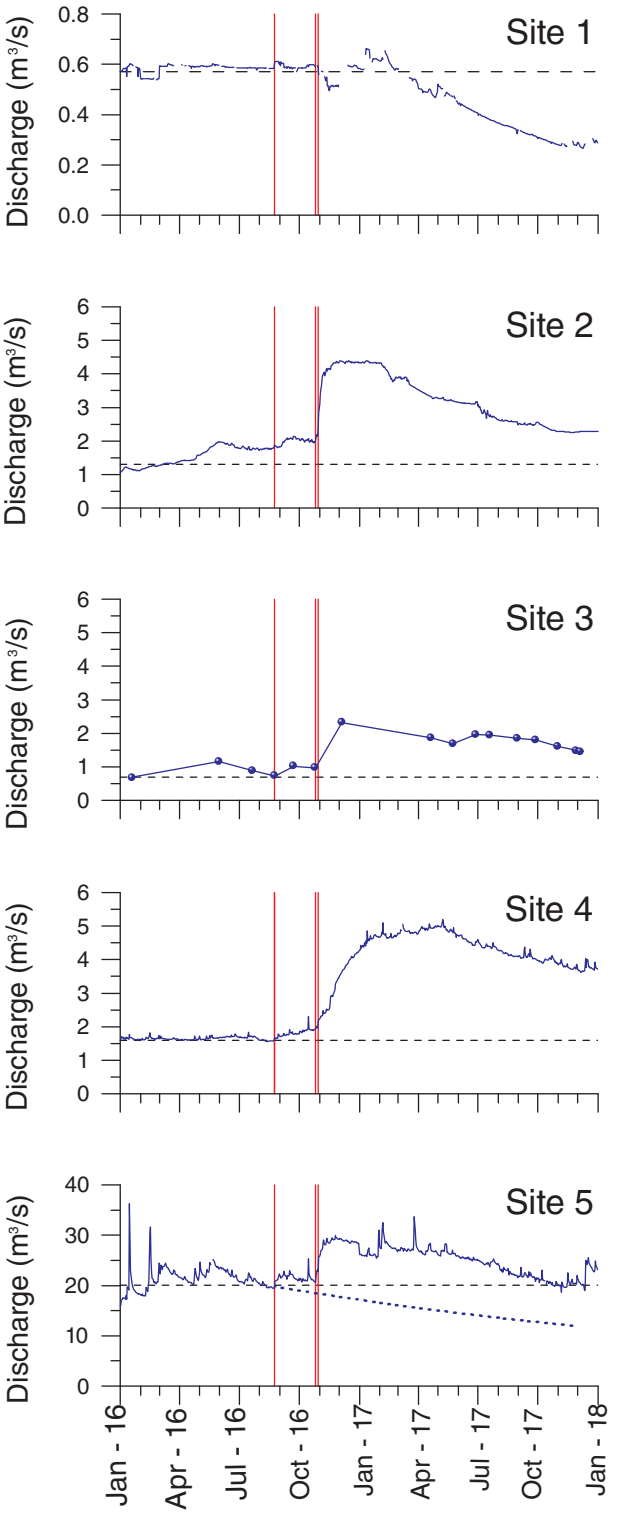

FIGURE 4 Daily discharge (m^3/s) of the monitoring sites in the 2016–2017 period. Vertical red bars locate the three main seismic events. The horizontal dot line indicates the pre-events mean discharge, reported in Table 1. In Site 3 graph, the spot discharge measurements are indicated (blue dots). In Site 5 graph, the recession curve (blue dotted line) is shown to identify the post-seismic surplus groundwater amount (RGA)

- Site 1 shows discharge instability in the 4 months following the events and a gradual and continued decrease in discharge since February 2017;
- Sites 2 and 5 show a much higher abrupt increase in discharge, followed by stability for 3 to 4 months. The discharge starts to decrease from February 2017 at Site 2 and from January 2017 at Site 5. In November 2017, only the Site 5 is the discharge reverted to the original value. The achievement of pre-earthquake conditions at Site 2, corresponding to a discharge of approximately 1.70 m^3/s, would be expected in April 2018 in the absence of seasonal recharge;
- the Site 3 response is similar to that of Site 2, but the lack of a continuous data set does not allow for an accurate evaluation;
- in Site 4, the discharge increases gradually and very considerably until January 2017. During the following months, the discharge continues to increase slightly and, from March to April, remains stable; since May, the discharge starts to drop staying above the pre-seismic average value. The zeroing of the earthquake effects on the Site 4 discharge (1.59 m^3/s) is forecasted in May 2020, not considering the effects of seasonal recharge.

The sustained seismic responses of the water table, monitored by the four piezometers at Site 2 (Figure 5, L) highlight a gradual rise in the water level for 2 months after the events, with the post-October rate of increase (between 3 and 8 m) significantly higher than the post-August rate (between 1 and 2 m). Immediately after the shocks, only the highest elevation piezometer (D) initially suffered from a sharp lowering, which was quickly balanced in the following days and later showed a significant rise. After December 2016, the water level decreases until November 2017, when the level stabilizes. After 1 year, the original values are still not fulfilled in the A, B, and C piezometers; only the D piezometer has attained a lower level than the pre-seismic condition.

The daily hydraulic gradient time patterns (Figure 5, R) mirror the daily water table trends overtime, and they highlight that post-August event increase has a negligible magnitude compared with the surplus amount related to the October events. Following the August shock, the mean gradient increased by 15% from 0.042 to 0.049, whereas the October events caused a 69% increase from 0.049 to 0.083. After December 3, 2016, the hydraulic gradient gradually decreased, reaching a steady-state condition in November 2017. The mean gradient stabilized at approximately 0.046 in the last days of November 2017, with a reduction of the abnormal spike of approximately 0.88%. The gradient stabilization could be referred to as a new hydraulic balance achievement, not excluding a possible meteoric recharge effect.

The AGA and RGA values are reported in Table 2, where the surplus/deficit amount (Δ) is expressed both in absolute values (m^3) and relative terms (percentage of the assumed value).

The post-seismic conditions of the August and October events are different not only for the groundwater discharge involved but also for the spatial distribution of their effects. The August event induced a general increase in the amount of groundwater outflow, both in the western (Sites 2, 3, and 4) and eastern (Site 1) sides of the study area. Even in the eastern sector, the percentage of the increase (2%) is one order of magnitude lower than that in the western side (approximately 20%). After the October events, in the western area, a sharp increase in groundwater amount (between 130% and 190%) was observed; conversely, the eastern side recorded a decrease of approximately 20%.

In the western sector of the VSM system, the seismic response difference between the two events is more evident. After the August event, the surplus amount of Site 5 is 30.7×10^6 m^3. The sum of the groundwater surplus of Sites 2, 3, and 4 is 4.5×10^6 m^3, corresponding to 15% of the Site 5 surplus. This rate is similar to the percentage of the baseflow measured at Site 5 and ascribed to the total spring discharge at Sites 2, 3, and 4 (17%). After the October events, a surplus of 407×10^6 m^3 was calculated at Site 5. The sum of the surplus of Sites 2, 3, and 4 is 183×10^6 m^3, which is equivalent to 45% of the Site 5 surplus. Thus, the October seismic effects are more localized and stronger in the springs at the study sites than at other sites.

The comparison of the hourly Upper Nera hydrograph discharge and the 12-hr hydraulic gradient calculated between the D piezometer and San Chiodo spring at Site 2 (Figure 6) highlights that the Upper Nera discharge increases by 9% after approximately 20 hr during the August event (Figure 6a), with a depletion of the hydraulic gradient

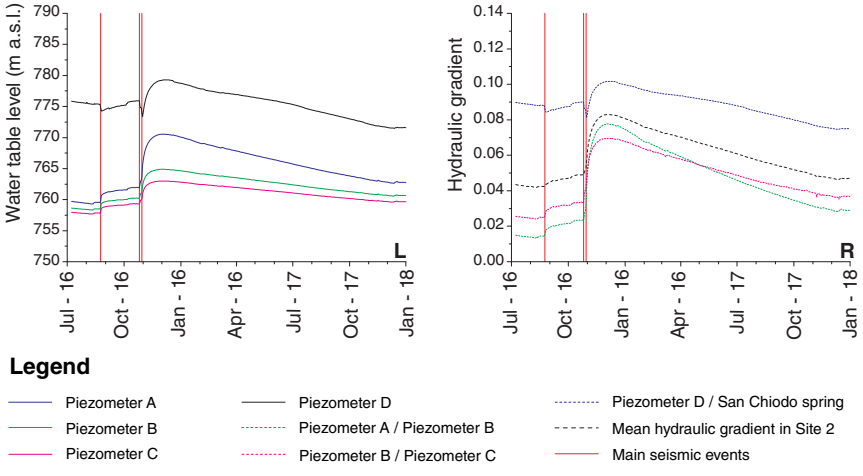

FIGURE 5 Daily hydrographs of water table levels (L) and hydraulic gradient "i" (R) at Site 2

TABLE 2 – Groundwater volumes involved in the 2016 seismic sequence related to two specified periods, corresponding to post-seismic condition of each seismic event

		August 24, 2016–October 25, 2016				October 26, 2016–November 30, 2017			
Site		AGA (10^6 m^3)	RGA (10^6 m^3)	Δ (10^6 m^3)	Δ (%)	AGA (10^6 m^3)	RGA (10^6 m^3)	Δ (10^6 m^3)	Δ (%)
1	Foce spring	3.17	3.22	0.05	2	20.40	16.55	- 3.85	19
2	Upper Nera River	9.22	11.02	1.80	20	40.20	116.42	76.22	190
3	Ussita River	3.83	5.04	1.21	32	25.48	65.82	40.34	158
4	Sordo River	8.65	10.18	1.53	18	54.54	124.47	69.93	123
5	Nera River (TO)	102.51	133.21	30.70	30	500.41	907.60	407.19	81

Abbreviations: AGA, assumed groundwater amount calculated in absence of the earthquakes; RGA, real groundwater amount involved; Δ, surplus /deficit amount expressed both in absolute values (m^3) and in percentage of the AGA.

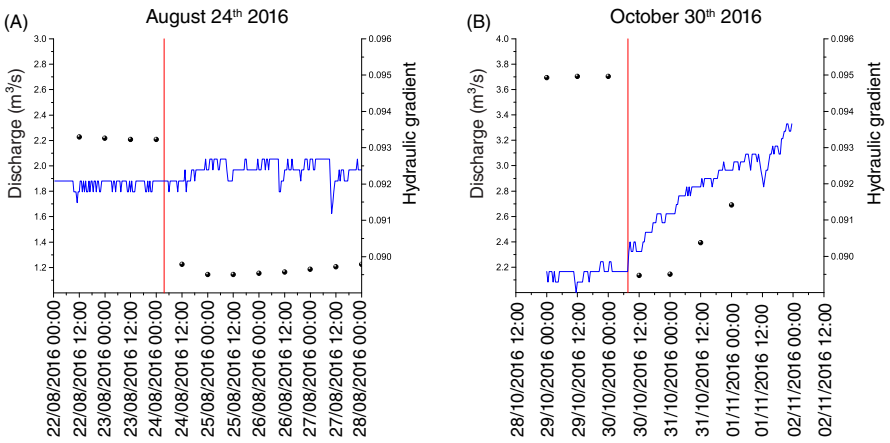

FIGURE 6 Discharge (blue line) versus hydraulic gradient (black dots) between the D piezometer and San Chiodo spring, recorded at Site 2, during August (a) and October (b). The red vertical line shows the time of the earthquake

TABLE 3 Terms of Darcy law evaluated in pre- and post-seismic conditions, for each seismic event

Event	Pre-seismic *i*	Post-seismic *i*	Pre-seismic *Q* (m^3/s)	Post-seismic *Q* (m^3/s)	Pre-seismic *KA* (m^3/s)	Post-seismic *KA* (m^3/s)	Δ*KA* (m^3/s)
August	0.0932	0.0895	1.88	2.05	20.17	22.91	2.73
October	0.0950	0.0895	2.16	2.40	22.74	26.82	4.08

Abbreviations: *i*, hydraulic gradient between D piezometer and San Chiodo spring; *Q*, discharge recorded in Site 2; *K*, hydraulic conductivity; *A*, cross-sectional area to flow; Δ*KA*: variation of *KA* value between pre and post conditions.

until 0.0895 occurring approximately 12 hr after the event. During the 4 days after the earthquake, the discharge and hydraulic gradient remained stable. The October events caused a 10% instantaneous increase in the discharge and a drop in the hydraulic gradient up to 0.0895, which began to rise 24 hr after the event (Figure 6b).

Darcy's law ($Q = KAi$) was applied to the hydraulic system of Site 2 in both pre- and post-event conditions (August and October; Table 3) to calculate the hydraulic conductivity enhancement. Q is the spring discharge (m^3/s), K is the hydraulic conductivity (m/s), A is the cross-sectional area to flow (m^2), and "i" is the hydraulic gradient between the D piezometer and San Chiodo spring.

Because the A value can be considered unchanged, the variation of the KA term can be attributed almost exclusively to K variation. Starting from this premise, even if the exact value of the K variation could not be assessed, the rate of permeability change with respect to its pre-event value has been evaluated.

At Site 2, the rate of permeability increase was estimated to be 13% and 19% of the pre-event values, for the August and October events, respectively. These increased values are lower than those reported in the literature, where a larger variability, between one and three times the order of magnitude, has been calculated (Rojstaczer et al., 1995; Tokunaga, 1999; Wang, Wang, Manga, Wang & Chen, 2013). After the two events, the rate of permeability increase is similar, and the mobilized groundwater amounts are very different, and it is necessary to find a further response mechanism for supporting the involvement of a large amount of groundwater during and after the October events.

7 | DISCUSSION

Within 2 months, the VSM hydrogeological system was affected by two main seismic events that were characterized by different

magnitudes and similar focal mechanisms and originated by the rupture of different segments of the same extensional tectonic element (VBF). Nevertheless, the two events produced different hydrogeological effects both in amplitude and spatial distribution.

The different responses would not seem to be associated with a different increase in permeability. In both seismic events, the flow rate increases, and the hydraulic gradient is reduced to 0.0895 (Figure 6) after the earthquake. In the case of the August earthquake, the hydraulic gradient and the flow rate remain stable at the new values for at least 4 days. In the October earthquake, the gradient and the range begin to progressively rise after 24 hr. The hydrogeological responses to both seismic events were a lowering of the hydraulic gradient up to the same value (0.0895) and an increase in the same percentage of discharge (9–10%). The identical responses are related to the similarity between the seismic events both in intensity (Mw 6.0–6.5) and in distances from the epicentre (Figure 1). The described aquifer responses fall within the interpretative models of enhanced permeability, due to the cleaning/widening of fractures. In extensional fractured carbonate systems, such as the one studied here, the short-term hydrogeological effects can be explained by the poroelastic response of the aquifer to the seismic perturbation, which creates a water mass imbalance and forces the water table to drop (Rojstaczer et al., 1995).

However, the significant increase in groundwater discharge recorded at the mid- and long-term can be attributed to cleaning and/or widening of the fractures, which cause enhancement of the permeability (Manga, 2001; Amoruso et al., 2011; Ingebritsen & Manning, 2010; Wang & Manga, 2015). The literature recognizes that poroelastic deformation contributes to a minor amount of water discharge compared with the permeability increase (Tokunaga, 1999; Manga et al., 2012).

The effect of the increase in permeability is quite clear after the August earthquake. In the following 2 months, the effect is uniformly distributed throughout the basal aquifer, thus producing persistent changes in the hydraulic features of the aquifer and resulting in a widespread and homogeneous increase in the discharge of all basal springs. The discharge surplus, linked to the effect of cleaning/widening of the fractures, should decrease according to the progressive closing of the fractures if further earthquakes do not occur. When the October earthquake occurred, the effect of the fracture widening related to the August earthquake does not seem to have been exhausted yet because the pre-earthquake conditions have not been restored at any monitoring site; therefore, the effects of the October earthquake would be superimposed to those of August. During the first 24 hr after the October 30 event, the increase in permeability was repeated with the same mechanism as the August earthquake, although with higher magnitude. Subsequently, a sudden and simultaneous increase in the hydraulic gradient and of the groundwater discharge was triggered. This abnormal response is unlikely to be explained by the sole increase in permeability.

A further interpretative conceptual model of the hydrogeological response to the seismic perturbation was carried out, to justify the significantly prolonged and localized overall groundwater discharge in the study system. We assumed that seismogenetic fault rupture might induce a disruption in the upgradient sector of the aquifer. The interpretation has similarities with the breaching hydraulic barriers or seals (Sibson, 1994; Brodsky et al., 2003; Wang et al., 2004). In central Apennine, a similar mechanism has been invoked for the first time (Saroli et al. 2012) for the Posta Fibreno fault with a progressive change in the base level of the groundwater flow with a related deepening of the karstic system. In the studied case, the trigger of the surplus groundwater transfer was not the removal of the temporary blockage in a fracture. The sudden formation of a displaced section area on the fault plane inside the saturated zone of the aquifer induced an abrupt hydraulic imbalance, favouring a surplus groundwater transfer through the newly displaced section. Owing to the described mechanism, named "Aquifer Fault Rupture" (AFR), the system will gradually tend to a new hydraulic equilibrium. The rate of the transient surplus discharge will start to decrease according to the hydraulic gradient drop. At the same time, the height of the wetted section will decrease, contributing to the consequential reduction of the surplus discharge. The new steady-state condition will be reached when the hydraulic gradient stabilizes and not necessarily when the surplus discharge decreases to zero, because the AFR mechanism might not be the only mechanism causing increase in the discharge.

The estimation of the "RGV" attributed to the AFR mechanism was partly based on the literature data. The broken plane of the VBF provides vertical offsets estimated at the mean depth of the basal water table at approximately 0.775 m on a fault segment approximately 20 km long, as explained above. The mean values of the hydraulic gradient range between 0.03 (Boni et al., 2005) and 0.04 (measured at Site 2); the hydraulic conductivity ranges between 2×10^{-2} and 4×10^{-2} m/s (Mastrorillo et al., 2012; Aquilanti et al., 2016).

The rate of the hydraulic gradient reduction over time is expressed by the exponential equation calculated for the mean gradient at Site 2 (Figure 5, R):

$$i = 0.0846e^{-0.002t}$$

where "i" is the hydraulic gradient value and "t" is the time in days.

The range of the increase in bulk permeability has been evaluated to be 13–19% with an average increase by 16%. The calculated average value of post-seismic permeability was estimated as approximately 3.5×10^{-2} m/s, which corresponds to the mean pre-seismic value of the above-mentioned literature and increased by 16%.

Starting from a mean VBF vertical offsets of approximately 0.775 m over the entire rupture plain (20 km), the mean displacement section was estimated to be 15.5×10^3 m^2. The application of Darcy's law, using the average values listed above, led to the estimation of the instantaneous groundwater surplus flow through the displaced section of approximately 19 m^3/s. Based on the assumption that the surplus discharge remains constant until the hydraulic gradient starts to decrease, the amount of the groundwater flow surplus, which occurred from October 31 until December 3, 2016, was evaluated at 53×10^6 m^3. After December 3, 2016, the amount of the

groundwater surplus flowing through the new displacement section area progressively decreased following the hydraulic gradient trend reduction until November 30, 2017. After this date, the hydraulic gradient stabilizes at a constant value of 0.047, which is 10% higher than the pre-seismic value (0.043). During December 3, 2016, to November 30, 2017, period, a groundwater flow surplus of 421×10^6 m^3 was calculated. Consequently, the total calculated groundwater flow surplus mobilized by the AFR mechanism is estimated to be approximately 474×10^6 m^3.

This interpretative conceptual model has been roughly validated by the comparison between the measured and calculated volumes of groundwater mobilized after the earthquakes. From November 1, 2016, until November 30, 2017, the 407×10^6 m^3 groundwater surplus measured at Site 5 is approximately similar to the groundwater flow surplus calculated through the VBF (474×10^6 m^3). The discrepancy is lower than 20% between the two inferred and observed volumes and can be attributed to the uncertainty of collected data and to errors in extrapolating permeability and hydraulic gradient from a local to regional scale. The temporal and spatial development of the proposed hydrodynamic response to the earthquake can be explained by the "basins-in-series system" (Petrella et al., 2009) interpretation of the VSM system (Figure 7). Immediately after the VBF surface rupture, a part of the total surplus groundwater transferred through the newly displaced section moving from east to west. The newly displaced section cuts the northern sector of Basin 2, producing a surplus of groundwater that reaches the springs at Site 2 and Site 3 almost instantaneously. Southward, the VBF cuts the western side of Basin 1, favouring a transfer of groundwater to Basin 2. This transfer triggers the translation and lowering of the groundwater divide between Basin 1 and Basin 2, with a consequent reduction in the discharge rate at Site 1 on the eastern side.

The inflow of the groundwater surplus in Basin 2 caused a rise in the water table, producing an increase in the groundwater flow already drained towards Basin 3 before the earthquakes. In Basin 3, the increased volume of groundwater transferred from Basin 2 leads to a rise in the water table at the Norcia Plain, an appearance of new springs (Console, Motti & Pantaleoni, 2017) and a progressive increase in the baseflow discharge at Site 4.

The hydrograph trends of the monitored sites (Figure 4) provide an idea of the temporal development of the described process. Site 2 shows a sudden increase in flow immediately after the October seismic events, with a shift of approximately 24 hr to the AFR movement. At Site 1, the progressive decrease in flow begins 4 months after the earthquake (February 2017), when the lowering of the surplus groundwater supplied by the springs at Sites 2 and 3 begins. At Site 4, the increase in spring discharge was growing smoothly; however, larger volumes of groundwater were affected. This evolution can be

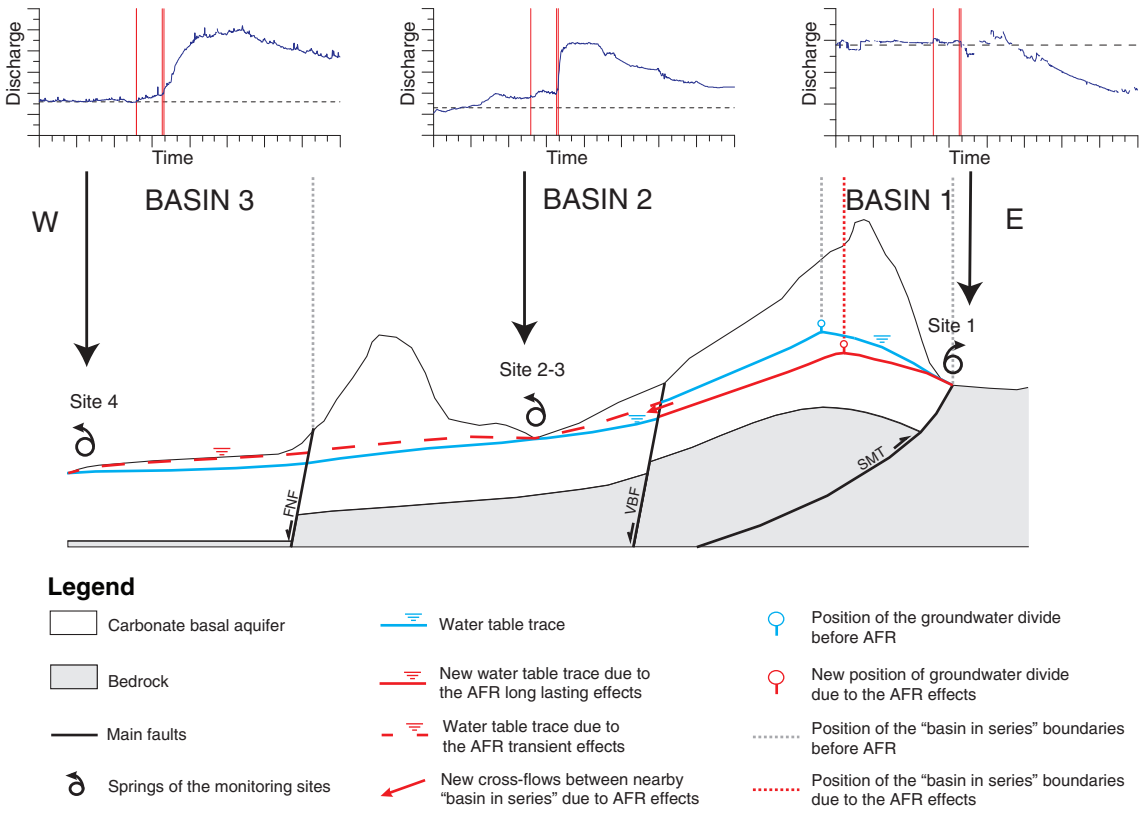

FIGURE 7 Schematic section showing the effects of the Aquifer Fault Rupture (AFR) mechanism on the basal aquifer of the Valnerina–Sibillini Mts. Hydrogeological system (VSM). This is an explanatory drawing not to scale and not matching to any trace in the hydrogeological map. Discharge graphs are related to Site 4, Site 2 and Site 1 (see Figure 4). The fault acronyms are explained in the legends of Figure 1 and Figure 2

related to the greater distance from the VBF and to the storage effect of the porous media in the Norcia plain aquifer. This smoothing effect would also be confirmed by the different values of the recession coefficient calculated in the post-earthquake conditions at Site 2 (0.003 d^{-1}) and Site 4 (0.001 d^{-1}), leading to different exhaustion times of the groundwater surplus. At Site 2, the surplus is expected to be exhausted by April 2018, whereas at Site 4, by May 2020.

8 | CONCLUSION

The study area, hosting large carbonate fractured hydrogeological systems, was affected by two main subsequent seismic events with magnitudes of 6.0 and 6.5, originating from the rupture of different segments of the same extensional VBF fault system. The hydrogeological responses to those seismic events exhibited significant differences both in the volume and in the persistence of the triggered groundwater surplus outflow. The second seismic event had the highest Mw (6.5) of the entire seismic sequence, and the amount of mobilized groundwater (approximately 400×10^6 m^3) was one order of magnitude higher than that of the previous amount (approximately 30×10^6 m^3). Such large induced variations in groundwater flow have also been observed 3 years after the earthquakes. Understanding that the largest event could amplify the not yet exhausted effects of the first event, the complex hydrogeological changes produced by the October 30 earthquake can be explained by conventional mechanisms described in the literature for similar cases.

Thorough analysis of the responses of this carbonate system revealed a strong dependence among hydrogeological anomalies, regional geological setting, and local seismogenetic processes. The combined study of these three topics allowed us to generate a new interpretative mechanism, named "Aquifer Fault Rupture" (AFR), which is able to explain the abnormal aquifer response to earthquakes. The proposed interpretation assumes that the seismogenetic fault rupture causes a disruption in the upgradient section of the aquifer, determining a sustained increase of the groundwater flow by increasing the hydraulic gradient in the aquifer. At the same time, this mechanism induces an additional westward/northward flow through the breaching of the pre-existing tectonic barrier and a shift eastward of the piezometric divide. The implication of this interpretation is supported by matching the results obtained from different quantitative evaluations. The calculated groundwater amount flowing through the new tectonic breaching (approximately 470×10^6 m^3) is consistent with the measured groundwater amount surplus outflowing from the whole regional basal aquifer.

Certainly, the obtained results of the hydrogeological response to earthquakes need to be refined. In fact, the observed changes in groundwater flow also have a long-term impact on groundwater management. In the studied system, the post-seismic position of the groundwater divide severely penalizes the eastern side of the Sibillini Mts., where even in the pre-seismic period, the mean total discharge of the springs (4.6 m^3/s) was far less than that of the western side (18.2 m^3/s). The proposed AFR model is unable to forecast if or when the modified piezometric divide would recover its original position. The existence of tapped sources of drinking water on the eastern side requires a careful evaluation of this issue, implying a revision of the long-term strategy to achieve sustainable management of groundwater resources.

The findings highlight the importance of the availability of a robust and widespread monitoring network to achieve significant quantitative results in earthquake hydrology. Classical hydrogeological data would not be sufficient if they are not compared with detailed geological setting and seismological data. In seismic areas hosting relevant groundwater resources, future development of combined hydrogeological and seismological monitoring networks is therefore considered highly recommended, at least with the aim of optimizing groundwater resource management.

ACKNOWLEDGEMENTS

Thanks go to the water supply companies S.A.N. (Macerata) and CIIP (Ascoli Piceno) for making the spring discharge and water table data freely available.

DATA AVAILABILITY STATEMENT

The data that support the findings of this study have been collected by Hydrographic Services of Umbria Region, water supply companies or directly from the research team. The data of the Umbria Region gauging stations network are available on request from from http://www.idrografico.regione.umbria.it/annali/. The data from the water supply companies are not publicly available due to privacy restrictions. The hydrological data collected from the research team are available from the corresponding author upon reasonable request.

ORCID

Lucia Mastrorillo https://orcid.org/0000-0003-3761-3719
Michele Saroli https://orcid.org/0000-0001-9499-3960
Stefano Viaroli https://orcid.org/0000-0002-2521-7463
Francesca Banzato https://orcid.org/0000-0001-8152-6247
Daniela Valigi https://orcid.org/0000-0002-2256-251X
Marco Petitta https://orcid.org/0000-0003-1137-6137

REFERENCES

Albano, M., Barba, S., Solaro, G., Pepe, A., Bignami, C., Moro, M., … Stramondo, S. (2017). Aftershocks, groundwater changes and postseismic ground displacements related to pore pressure gradients: Insights from the 2012 Emilia-Romagna earthquake. *Journal of Geophysical Research: Solid Earth*, *122*, 5622–5638. https://doi.org/10.1002/2017JB014009

Albano, M., Barba, S., Saroli, M., Polcari, M., Bignami, C., Moro, M., … Di Bucci, D. (2019). Aftershock rate and pore fluid diffusion: Insights from the Amatrice-Visso-Norcia (Italy) 2016 seismic sequence. *Journal of Geophysical Research: Solid Earth*, *124*, 995–1015. https://doi.org/10.1029/2018JB015677

Adinolfi, F. R., Carucci, V., Falgiani, A., Manetta, M., Parisse, B., Petitta, M., … Tallini, M. (2012). Changes on groundwater flow and hydrochemistry of the Gran Sasso carbonate aquifer after 2009 L'Aquila earthquake. *Italian Journal of Geosciences*, *131*(3), 459–474. https://doi.org/10.3301/IJG.2012.05

Amoruso, A., Crescentini, L., Petitta, M., Rusi, S., & Tallini, M. (2011). Impact of the April 6, 2009 L'Aquila earthquake on groundwater flow in the Gran Sasso carbonate aquifer Central Italy. *Hydrological Processes*, *25*(11), 1754–1764. https://doi.org/10.1002/hyp.7933

Aquilanti, L., Clementi, F., Nanni, T., Palpacelli, S., Tazioli, A., & Vivalda, P. M. (2016). DNA and fluorescein tracer tests to study the recharge, groundwater flowpath and hydraulic contact of aquifers in the Umbria-Marche limestone ridge (central Apennines, Italy). *Environmental Earth Sciences*, *75*(7), 626. https://doi.org/10.1007/s12665-016-5436-5

Barberio, M. D., Barbieri, M., Billi, A., Doglioni, C., & Petitta, M. (2017). Hydrogeochemical changes before and during the 2016 Amatrice-Norcia seismic sequence (Central Italy). *Scientific Reports*, *7*, 11735. https://doi.org/10.1038/s41598-017-11990-8

Bense, V. F., Gleeson, T., Loveless, S. E., Bour, O., & Scibek, J. (2013). Fault zone hydrogeology. *Earth-Science Reviews*, *127*, 171–192. https://doi.org/10.1016/j.earscirev.2013.09.008

Bigi, S., Casero, P., Chiarabba, C., & Di Bucci, D. (2012). Contrasting surface active faults and deep seismogenic sources unveiled by the 2009 L'Aquila earthquake sequence (Italy). *Terra Nova*, *25*, 21–29. https://doi.org/10.1111/ter.12000

Boni, C., Baldoni, T., Banzato, F., Cascone, D., & Petitta, M. (2010). Hydrogeological study for identification, characterization and management of groundwater resources in the Sibillini Mountains National Park (Central Italy). *Italian Journal of Engineering Geology and Environment*, *2*, 21–39. https://doi.org/10.4408/IJEGE.2010-02.O-02

Boni, C., Bono, P., & Capelli, G. (1986). Schema idrogeologico dell'Italia Centrale (Hydrogeological scheme of central Italy). *Memorie Della Societa Geologica Italiana*, *35*, 991–1012.

Boni C., Mastrorillo M., Cascone D. & Tarragoni C. (2005). Carta idrogeologica delle dorsali interne umbro-marchigiane (scala 1:50.000). *Pubblicazione N° 2865 CNR – Gruppo Nazionale Difesa Catastrofi Idrogeologiche*

Brodsky, E. E., Roeloffs, E. A., Woodcock, D., Gall, I., & Manga, M. (2003). A mechanism for sustained ground water pressure changes induced by distant earthquakes. *Journal of Geophysical Research: Solid Earth*, *108*(8), ESE7/1–ESE7/10. https://doi.org/10.1029/2002JB002321

Brozzetti, F., Boncio, P., Cirillo, D., Ferrarini, F., de Nardis, R., Testa, A., … Lavecchia, G. (2019). High-resolution field mapping and analysis of the August–October 2016 coseismic surface faulting (Central Italy earthquakes): Slip distribution, parameterization, and comparison with global earthquakes. *Tectonics*, *38*, 417–439. https://doi.org/10.1029/2018TC005305

Calamita, F., Cello, G., Deiana, G., & Paltrinieri, W. (1994). Structural styles, chronology-rates of deformation and time space relationships in the Umbria-Marche thrust system (central Apennines, Italy). *Tectonics*, *13*, 873–881. https://doi.org/10.1029/94TC00276

Calamita, F., Coltorti, M., Farabollini, P., & Pizzi, A. (1994). Le faglie normali quaternarie della dorsale appenninica umbro-marchigiana: proposta di un modello di tettonica di inversione. *Studi Geologici Camerti*, *1994*, 211–225.

Calamita, F., & Deiana, G. (1988). The arcuate shape of the Umbria-Marche Apennines (Central Italy). *Tectonophysics*, *146*, 139–147. https://doi.org/10.1016/0040-1951(88)90087-X

Calamita, F., & Pizzi, A. (1993). Tettonica quaternaria nella dorsale appenninica umbro-marchigiana e bacini intrappenninici associati. *Studi Geologici Camerti*, *1992*(1), 17–26.

Carro, M., Amicis, M. D., & Luzi, L. (2005). Hydrogeological changes related to the Umbria–Marche earthquake of September 26, 1997 (Central Italy). *Natural Hazards*, *34*, 315–339. https://doi.org/10.1007/s11069-004-2074-0

Casini, S., Martino, S., Petitta, M., & Prestininzi, A. (2006). A physical analogue model to analyse interactions between tensile stresses and dissolution in carbonate slopes. *Hydrogeology Journal*, *14*(8), 1387–1402. https://doi.org/10.1007/s10040-006-0064-x

Cavinato, G. P., & De Celles, P. G. (1999). Extensional basins in the tectonically bimodal central Apennines fold-thrust belt, Italy: Response to corner flow above a subducting slab in retrograde motion. *Geology*, *27*, 956–959. https://doi.org/10.1130/0091-7613(1999)027<0955:EBITTB>2.3.CO;2

Centamore, E., Rossi, D., & Tavarnelli, E. (2009). Geometry and kinematics of Triassic to recent structures in the northern-central Apennines: A review and an original working hypothesis. *Italian Journal of Geosciences*, *128*, 419–432. https://doi.org/10.3301/IJG.2009.128.2.419

Checcucci, R., Mastrorillo, L., & Valigi, D. (2017). Groundwater and earthquake: Brief remarks about seismic effects on groundwater resources availability in Valnerina. *Italian Journal of Groundwater*, *6*, 75–77. https://doi.org/10.7343/as-2017-259

Cheloni, D., De Novellis, V., Albano, M., Antonioli, A., Anzineu, M., Atzori, S., … Doglioni, C. (2017). Geodetic model of the 2016 Central Italy earthquake sequence inferred from InSAR and GPS data. *Geophysical Research Letters*, *44*, 6778–6787. https://doi.org/10.1002/2017GL073580

Cheloni, D., Falcucci, E., & Gori, S. (2019). Half-graben rupture geometry of the October 30, 2016 MW 6.6 Mt. Vettore-Mt. Bove earthquake, Central Italy. *Journal of Geophysical Research: Solid Earth*, *124*, 4091–4118. https://doi.org/10.1029/2018JB015851

Cheloni, D., Giuliani, R., D'Anastasio, E., Atzoria, S., Walters, J., Bonci, L., … Stefanelli, G. (2014). Coseismic and post-seismic slip of the 2009 L'Aquila (Central Italy) Mw 6.3 earthquake and implications for seismic potential along the Campotosto fault from joint inversion of high-precision levelling, InSAR and GPS data. *Tectonophysics*, *622*, 168–185. https://doi.org/10.1016/j.tecto.2014.03.009

Chiaraluce, L., Di Stefano, R., Tinti, E., Scognamiglio, L., Michele, M., Casarotti, E., … Marzorati, S. (2017). The 2016 Central Italy seismic sequence: A first look at the mainshocks, aftershocks, and source models. *Seismological Research Letters*, *88*(3), 757–771. https://doi.org/10.1785/0220160221

Chiaraluce, L., Valoroso, L., Piccinini, D., Di Stefano, R., & De Gori, P. (2011). The anatomy of the 2009 L'Aquila normal fault system (Central Italy) imaged by high resolution foreshock and aftershock locations. *Journal of Geophysical Research:Solid Earth*, *116*(B12311), 1–25. https://doi.org/10.1029/2011JB008352

Civico, R., Pucci, S., Villani, F., Pizzimenti, L., De Martini, P. M., et al. (2018). The open EMERGEO working group (2018) surface ruptures following the October 30, 2016 Mw 6.5 Norcia earthquake, Central Italy. *Journal of Maps*, *14*(2), 151–160. https://doi.org/10.1080/17445647.2018.1441756

Claesson, L., Skelton, A., Graham, C., Dietl, C., Mörth, M., Torssander, P., & Kockum, I. (2004). Hydrogeochemical changes before and after a major earthquake. *Geology*, *32*, 641–644. https://doi.org/10.1130/G20542.1

Coltorti, M., & Farabollini, P. (1995). Quaternary evolution of the. *Castelluccio di Norcia Basin (Umbro-Marchean Apennines, Italy) Il Quaternario Italian Journal of Quaternary Sciences*, *8*(1), 149–166.

Console, F., Motti, A., & Pantaloni, M. (2017). L'intermittenza delle sorgenti del Torbidone nella Piana di Norcia: analisi delle fonti storiche a partire dal XIV secolo. *Rendiconti Online Della Società Geologica Italiana*, *43*, 38–58. https://doi.org/10.3301/ROL.2017.34

Cooper, H. H., Bredehoeft, J. D., Papadopulos, I. S., & Bennett, R. R. (1965). The response of well–aquifer systems to seismic waves. *Journal of Geophysical Research: Solid Earth*, *70*, 3915–3926.

Doglioni, C., Carminati, E., Cuffaro, M., & Scrocca, D. (2007). Subduction kinematics and dynamic constraints. *Earth-Science Reviews*, *83*, 125–175. https://doi.org/10.1016/j.earscirev.2007.04.001

Elkhoury, J. E., Brodsky, E. E., & Agnew, D. C. (2006). Seismic waves increase permeability. *Nature*, *441*, 1135–1138. https://doi.org/10.1038/nature04798

EMERGEO Working Group (2016). Terremoto di Amatrice del 24 agosto 2016: Effetti Cosismici doi: https://doi.org/10.5281/zenodo.61566

Esposito, E., Pece, R., Porfido, S., & Tranfaglia, G. (2001). Hydrological anomalies connected to earthquakes in southern Apennines (Italy). *Natural Hazards and Earth System Sciences*, *1*(3), 137–144. https://doi.org/10.5194/nhess-1-137-2001

Esposito, E., Pece, R., Porfido, S., & Tranfaglia, G. (2009). Ground effects and hydrological changes in the southern Apennines (Italy) in response to the July 23, 1930 earthquake (MS=6.7). *Natural Hazards and Earth System Sciences*, *9*, 539–550. https://doi.org/10.5194/nhess-9-539-2009

Galadini, F., Falcucci E., Gori S., Kayen R. E., Lingwall B., Pizzi A., … & Stewart J. P. (2017) Chapter 2: Seismic source and surface rupture, in engineering reconnaissance following the 2016 Central Italy earthquakes. *Geotechnical Extreme Events Reconnaissance Association Report no. GEER-050D*, 33–50, Zimmaro P. and Stewart J.P. Eds. https://doi.org/10.18118/G6HS39

Galassi, D. M., Lombardo, P., Fiasca, B., Di Cioccio, A., Di Lorenzo, T., Petitta, M., & Di Carlo, P. (2014). Earthquakes trigger the loss of groundwater biodiversity. *Scientific Reports - Nature*, *4*, 6273. https://doi.org/10.1038/srep06273

Giacopetti M., Fabbrocino S., Ianni C., Materazzi M., & Pambianchi G. (2019) Co-seismic and post-seismic changes in groundwater discharge: First results from the epicentral region of the Central Italy earthquake 2016 *Rendiconti Online Della Società Geologica Italiana 47*, 52–57, 3 https://doi.org/10.3301/ROL.2019.10

Huang, M. H., Fielding, E. J., Liang, C., Milillo, P., Bekaert, D., Dreger, D., & Salzer, J. (2017). Coseismic deformation and triggered landslides of the 2016 Mw 6.2 Amatrice earthquake in Italy. *Geophysical Research Letters*, *44*, 1266–1274. https://doi.org/10.1002/2016GL071687

Ingebritsen, S. E., & Manning, C. E. (2010). Permeability of the continental crust: Dynamic variations inferred from seismicity and metamorphism. *Geofluids*, *10*, 193–205. https://doi.org/10.1111/j.1468-8123.2010.00278.x

IRSA-CNR (2017). Caratterizzazione climatica del regime pluviometrico nell'area del Distretto Idrografico dell'Appennino centrale nel periodo 1951–2017. http://www.irsa.cnr.it/index.php/ita/news/item/192-report-regime-climatico

Jonsson, S., Segall, P., Pedersen, R., & Bjornsson, G. (2003). Post-earthquake ground movements correlated to pore-pressure transients. *Nature*, *424*(6945), 179–183. https://doi.org/10.1038/nature01776

Kim, J., Lee, J., Petitta, M., Kim, H., Kaown, D., Para, I. W., … Lee, K. K. (2019). Groundwater system responses to the 2016 ML 5.8 Gyeongju earthquake, South Korea. *Journal of Hydrology*, *576*, 150–163. https://doi.org/10.1016/j.jhydrol.2019.06.044

Lachassagne, P., Leonardi, V., Vittecoq, B., & Henriot, A. (2011). Interpretation of the piezometric fluctuations and precursors associated with the November 29, 2007, magnitude 7.4 earthquake in Martinique (lesser Antilles). *Comptes Rendus Geoscience Journal*, *343*, 760–776. https://doi.org/10.2016/j.crte.2011.09.002

Lavecchia, G., Castaldo, R., de Nardis, R., de Novellis, V., Ferrarini, F., Pepe, S., … Tizzani, P. (2016). Ground deformation and source geometry of the August 24, 2016 Amatrice earthquake (Central Italy) investigated through analytical and numerical modeling of DInSAR measurements and structural-geological data. *Geophysical Research Letters*, *43*(24), 12,389–12,398. https://doi.org/10.1002/2016GL071723

Leggette, R. M., & Taylor, G. H. (1935). Earthquakes instrumentally recorded in artesian wells. *Bulletin of Seismological Society of America*, *25*, 169–175.

Liberatore, D., Doglioni, C., AlShawaa, O., Atzorib, S., & Sorrentino, L. (2019). Effects of coseismic ground vertical motion on masonry constructions damage during the 2016 Amatrice-Norcia (Central Italy) earthquakes. *Soil Dynamics and Earthquake Engineering*, *120*, 423–435. https://doi.org/10.1016/j.soildyn.2019.02.015

Luzi, L., D'Amico, M., Massa, M., & Puglia, R. (2018). Site effects observed in the Norcia intermountain basin (Central Italy) exploiting a 20-year monitoring. *Bulletin of Earthquake Engineering*., *17*, 97–118. https://doi.org/10.1007/s10518-018-0444-3

Maillet, E. (1905). *Essais d'hydraulique souterraine et fluviale* (p. 218). Hermann, Paris: Ed. Librairie Scientifique A.

Manga, M. (2001). Origin of postseismic streamflow changes inferred from baseflow recession and magnitude-distance relation. *Geophysical Research Letters*, *28*(10), 2133–2136. https://doi.org/10.1029/2000GL012481

Manga, M., Beresnev, I., Brodsky, E. E., Elkhoury, J. E., Elsworth, D., Ingebritsen, S. E., … Wang, C. Y. (2012). Changes in permeability caused by transient stresses: Field observations, experiments, and mechanisms. *Reviews of Geophysics*, *50*(RG2004), 1–24.

Manga M., Brodsky E.E. & Boone M. (2003). Response of stream flow to multiple earthquakes. *Geophysical Research Letters 30* (5,1214). 18–1 – 18-4. doi:https://doi.org/10.1029/2002GL016618, 2003

Manga, M., & Rowland, J. C. (2009). Response of alum rock springs to the October 30, 2007 alum rock earthquake and implications for the origin of increased discharge after earthquakes. *Geofluids*, *9*(3), 237–250. https://doi.org/10.1111/j.1468-8123.2009.00250.x

Mastrorillo, L. (2001). Elementi strutturali e caratteristiche idrogeologiche della dorsale carbonatica Umbro-Marchigiana interna. *Memorie Della Societa Geologica Italiana*, *56*, 219–226.

Mastrorillo, L., Baldoni, T., Banzato, F., Boscherini, A., Cascone, D., Checcucci, R., … Boni, C. (2009). Quantitative hydrogeological analysis of the carbonate domain of the Umbria region (Central Italy). *Italian Journal of Engineering Geology and Environment*, *1*, 137–155.

Mastrorillo, L., Nanni, T., Petitta, M., Vivalda, P. M., Banzato, F., & Palpacelli, S. (2012). Groundwater resources of the Upper Basin of Aso River (Sibillini Mts. National Park): Hydrogeological study and management evaluation. *Engineering-Hydro-Environmental Geology (Giornale di Geologia Applicata)*, *15*, 83–96. https://doi.org/10.1474/EHEGeology.2012-15.0-06.0296

Mastrorillo, L., & Petitta, M. (2010). Effective infiltration variability in the Umbria-Marche carbonate aquifers of Central Italy. *Journal of Mediterranean Earth Sciences*, *2*, 9–18. https://doi.org/10.3304/JMES.2010.002

Mastrorillo, L., & Petitta, M. (2014). Hydrogeological conceptual model of the upper Chienti River basin aquifers (Umbria-Marche Apennines). *Italian Journal of Geoscience*, *133*(3), 396–408. https://doi.org/10.3301/IJG.2014.12

Mogi K., Mochizuki H. & Kurokawa Y. (1989) Temperature changes in an artesian spring at Usami in the Izu peninsula (Japan) and their relation to earthquakes. *Tectonophysics Journal 159*(1–2), 95–108. https://doi.org/10.1016/0040-1951(89)90172-8

Mohr, C. H., Manga, M., Wang, C. Y., Kirchner, J. W., & Bronstert, A. (2015). Shaking water out of soil. *Geology*, *43*(3), 207–210. https://doi.org/10.1130/G36261.1

Montgomery, D. R., & Manga, M. (2003). Streamflow and water well responses to earthquakes. *Science*, *300*(5628), 2047–2049. https://doi.org/10.1126/science.1082980

Muir-Wood, R., & King, G. C. P. (1993). Hydrological signatures of earthquake strain. *Journal of Geophysical Research: Solid Earth*, *98*, 22035–22068. https://doi.org/10.1029/93JB02219

Nanni, T., & Vivalda, P. (2005). The aquifers of the Umbria-Marche Adriatic region: Relationships between structural setting and groundwater chemistry. *Italian Journal of Geosciences*, *124*, 523–542.

Petitta M. (2011) Integrazione della base conoscitiva per la gestione della risorsa idrica sotterranea del Parco Nazionale dei Monti Sibillini. Tecnical Report for internal use. Parco Nazionale dei Monti Sibillini, p. 101

Petitta, M., Mastrorillo, L., Preziosi, E., Banzato, F., Barberio, D. M., Billi, A., … Doglioni, C. (2018). Water-table and discharge changes associated with the 2016–2017 seismic sequence in Central Italy: Hydrogeological data and a conceptual model for fractured carbonate aquifers. *Hydrogeology Journal*, *26*, 1009–1026. https://doi.org/10.1007/s10040-017-1717-7

Petrella, E., Capuano, P., Carcione, M., & Celico, F. (2009). A high-altitude temporary spring in a compartmentalized carbonate aquifer: The role

of low-permeability faults and karst conduits. *Hydrological. Processes*, *23*, 3354–3364. https://doi.org/10.1002/hyp.7454

Pierantoni, P., Deiana, G., & Galdenzi, S. (2013). Stratigraphic and structural features of the Sibillini mountains (Umbria-Marche Apennines, Italy). *Italian Journal of Geosciences*, *132*(3), 497–520. https://doi.org/10.3301/IJG.2013.08

Pizzi, A., Di Domenica, A., Gallovič, F., Luzi, L., & Puglia, R. (2017). Fault segmentation as constraint to the occurrence of the main shocks of the 2016 Central Italy seismic sequence. *Tectonics*, *36*, 1–18. https://doi.org/10.1002/2017TC004652

Pizzi, A., & Scisciani, V. (2000). Methods for determining the Pleistocene-Holocene component of displacement on active faults reactiving pre-Quaternary structures: Examples from the central Apennines (Italy). *Journal of Geodynamics*, *29*(3), 445–457. https://doi.org/10.1016/S0264-3707(99)00053-8

Pucci, S., De Martini, P. M., Civico, R., Nappi, R., Ricci, T., Villani, F., … Lancia, M. (2016). Coseismic effects of the 2016 Amatrice seismic sequence: First geological results. Annals of geophysics 59. *Fast Track*, *5*, 1–8. https://doi.org/10.4401/ag-7195

Roeloffs, E. A. (1998). Persistent water level changes in a well near Parkfield, California, due to local and distant earthquakes. *Journal of Geophysical Research: Solid Earth*, *103*(1), 869–889.

Rojstaczer, S., Wolf, S., & Michel, R. (1995). Permeability enhancement in the shallow crust as a cause of earthquake-induced hydrological changes. *Nature*, *373*(6511), 237–239. https://doi.org/10.1038/373237a0

Rosen, M. R., Binda, G., Archer, C., Pozzi, A., Michetti, A. M., & Noble, P. J. (2018). Mechanisms of earthquake-induced chemical and fluid transport to carbonate groundwater springs after earthquakes. *Water Resources Research*, *54*, 5225–5244. https://doi.org/10.1029/2017WR022097

Saroli, M., Albano, M., Giovinco, G., Casale, A., Dell'Isola, M., … Petitta, M. (2019). A macroscale hydrogeological numerical model of the Suio Hydrothermal System (Central Italy). *Geofluids*, *2019*, 5485068. https://doi.org/10.1155/2019/5485068

Saroli, M., Moro, M., Gori, S., Falcucci, E., & Salvatore, M. C. (2012). Tettonica, idrogeologia e carsismo: un nuovo approccio multidisciplinare per lo studio della tettonica attiva. L'esempio della faglia di Posta Fibreno (Marsica occidentale-Lazio Meridionale). *Italian Journal of Engineering Geology and Environment*, *14B*, 215–216. https://doi.org/10.1474/EHEGeology.2012-14.B.160

Scognamiglio, L., Tinti, E., Casarotti, E., Pucci, S., Villani, F., Cocco, M., … Dreger, D. (2018). Complex fault geometry and rupture dynamics of the MW 6.5, October 30, 2016, Central Italy earthquake. *Journal of Geophysical Research: Solid Earth*, *123*, 2943–2964. https://doi.org/10.1002/2018JB015603

Shi, Z., Wang, G., Manga, M., & Wang, C. Y. (2015). Continental-scale water level response to a large earthquake. *Geofluids*, *15*(1–2), 310–320. https://doi.org/10.1111/gfl.12099

Sibson, R. H. (1994). Crustal stress, faulting and fluid flow. *Geological Society London Special Publications*, *78*, 69–84. https://doi.org/10.1144/GSL.SP.1994.078.01.07

Sibson, R. H., & Rowland, J. (2003). Stress, fluid pressure and structural permeability in seismogenic crust, North Island, New Zealand. *Geophysical Journal International*, *154*(2), 584–594. https://doi.org/10.1046/j.1365-246X.2003.01965.x

Skelton, A., Andrén, M., Kristmannsdóttir, H., Stockmann, G., Mörth, C. M., Sveinbjörnsdóttir, Á., … Kockum, I. (2014). Changes in groundwater chemistry before two consecutive earthquakes in Iceland. *Nature Geoscience*, *7*(10), 752–756. https://doi.org/10.1038/NGEO2250

Tavani, S., Storti, F., Bausà, J., & Muñoz, J. A. (2012). Late thrusting extensional collapse at the mountain front of the northern Apennines (Italy). *Tectonics*, *31*(4), TC4019. https://doi.org/10.1029/2011TC003059

Tinti, E., Scognamiglio, L., Michelini, A., & Cocco, M. (2016). Slip heterogeneity and directivity of the ML 6.0, 2016, Amatrice earthquake estimated with rapid finite-fault inversion. *Geophysical Research Letters*, *43*, 745–752. https://doi.org/10.1002/2016GL071263

Tokunaga, T. (1999). Modeling of earthquake-induced hydrological changes and possible permeability enhancement due to the January 17, 1995 Kobe earthquake, Japan. *Journal of Hydrology*, *223*, 221–229.

Tung, S., & Masterlark, T. (2018). Delayed poroelastic triggering of the 2016October Visso earthquake by the August Amatrice earthquake, Italy. *Geophysical Research Letters*, *45*, 2221–2229. https://doi.org/10.1002/2017GL076453

Valerio, E., Tizzani, P., Carminati, E., Doglioni, C., Pepe, S., Petricca, P., … Lanari, R. (2018). Ground deformation and source geometry of the October 30, 2016 Mw 6.5 Norcia earthquake (Central Italy) investigated through seismological data, DInSAR measurements, and numerical modelling. *Remote Sensing*, *10*(12), 19. https://doi.org/10.3390/rs10121901

Valigi, D., Mastrorillo, L., Cambi, C., Barchi, M. R., Cardellini, C., Checcucci, R., … Vispi, I. (2019). Springs discharge variations induced by strong earthquakes: The Mw 6.5 Norcia event (Italy, October 30th 2016). *Rendiconti Online Della Società Geologica Italiana*, *47*, 141–146. https://doi.org/10.3301/ROL.2019.25

Villani, F., Sapia, V., Baccheschi, P., Civico, R., Di Giulio, G., Vassallo, M., … Pantosti, D. (2019). Geometry and structure of a fault-bounded extensional basin by integrating geophysical surveys and seismic anisotropy across the October 30, 2016 Mw 6.5 earthquake fault (Central Italy): The Pian Grande di Castelluccio basin. *Tectonics*, *38*, 26–48. https://doi.org/10.1029/2018TC005205

Wakita, H. (1975). Water wells as possible indicators of tectonic strain. *Science*, *189*(4202), 553–555. https://doi.org/10.1126/science.189.4202.553

Walters, R. J., Gregory, L. C., Wedmoreb, L. N. J., Craig, T. J., McCaffrey, K., Wilkinson, M., … Vittori, E. (2018). Dual control of fault intersections on stop-start rupture in the 2016 Central Italy seismic sequence. *Earth and Planetary Science Letters*, *500*, 1–14. https://doi.org/10.1016/j.epsl.2018.07.043

Wang, C. Y., & Manga, M. (2010). Earthquakes influenced by water. *Lecture Notes in Earth Sciences*, *114*, 125–139. https://doi.org/10.1007/978-3-642-00810-8_8

Wang, C. Y., & Manga, M. (2015). New streams and springs after the 2014 Mw6.0 South Napa earthquake. *Nature Communications*, *6*, 7597. https://doi.org/10.1038/ncomms8597

Wang, C. Y., Wang, C. H., & Kuo, C. H. (2004). Temporal change in groundwater level following the 1999 (mw 7.5) chi-chi earthquake, Taiwan. *Geofluids*, *4*(3), 210–220. https://doi.org/10.1111/j.1468-8123.2004.00082.x

Wang, C. Y., Wang, C. H., & Manga, M. (2004). Coseismic release of water from mountains: Evidence from the 1999 (mw=7.5) chi-chi, Taiwan, earthquake. *Geology*, *32*, 769–772. https://doi.org/10.1130/G20753.1

Wang, C. Y., Wang, L. P., Manga, M., Wang, C. H., & Chen, C. H. (2013). Basin-scale transport of heat and fluid induced by earthquakes. *Geophysical Research Letters*, *40*(15), 3893–3897. https://doi.org/10.1002/grl.50738

Yan, R., Woith, H., & Wang, R. (2014). Groundwater level changes induced by the 2011 Tohoku earthquake in China mainland. *Geophysical Journal International*, *199*(1), 533–548. https://doi.org/10.1093/gji/ggu196

How to cite this article: Mastrorillo L, Saroli M, Viaroli S, Banzato F, Valigi D, Petitta M. Sustained post-seismic effects on groundwater flow in fractured carbonate aquifers in Central Italy. *Hydrological Processes*. 2020;34:1167–1181. https://doi.org/10.1002/hyp.13662